Supplementary Information

NMDA spikes enhance action potential generation during sensory input

Lucy M. Palmer, Adam S. Shai, James E. Reeve, Harry L. Anderson, Ole Paulsen, Matthew E. Larkum

Nature Neuroscience: doi:10.1038/nn.3646

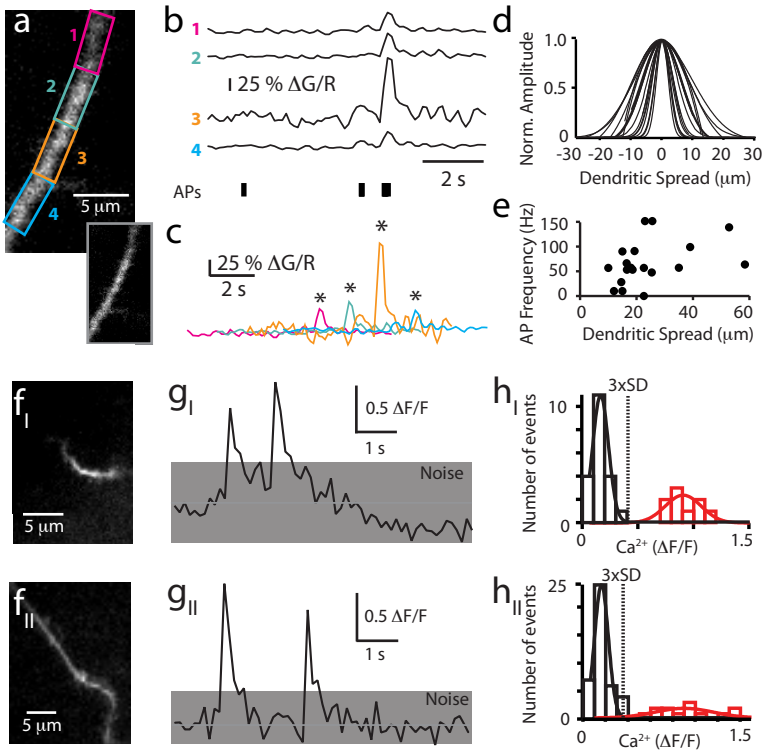

Supplementary Figure 1. Tuft Ca^{2+} transients are spatially restricted, have a distinct bimodal distribution, and are not graded in amplitude. In principle, NMDA spikes in multiple branches could be an indication of many NMDA spikes or one very spatially distributed NMDA event. We therefore measured the spatial extent of tuft Ca^{2+} transients. **(a)** Two-photon image of a tuft dendrite with spatially restricted regions of interest (ROIs; 5 µm length; coloured boxes). **(b)** Spontaneous Ca^{2+} transients recorded in the dendritic ROIs shown in (a) and somatic APs indicated by dashes. To compare different dendritic regions, transients are reported as ΔG/R. **(c)** Overlay of the transients in (b) illustrating the spread of a Ca^{2+} event along a tuft dendrite. **(d)** Gaussian distribution of the normalized Ca^{2+} transient amplitudes at different locations along tuft dendrites. **(e)** The spatial spread of the Ca^{2+} transients within a tuft dendrite was not related to the somatic AP firing frequency. **(f-h)** Since NMDA spikes have a clear threshold, plotting Ca^{2+} fluorescence amplitudes would result in a bimodal distribution whereas boosted potentials would have a graded distribution. We therefore plotted the Ca^{2+} fluorescence amplitude distributions from two example tuft dendrites (I and II). **(f)** Two-photon image of two example tuft dendrites. **(g)** Example fluorescence traces with two Ca^{2+} transients above the noise from tuft dendrite shown in (f). **(h)** Histogram of the peak amplitude of Ca^{2+} fluorescence from the tuft dendrite shown in (f) illustrating bimodal distributions. Ca^{2+} transients were included in the analysis if they had an amplitude larger than 3x the standard deviation of the noise (middle, grey bar; right, dashed line). This criteria separated the reported Ca^{2+} transients (red) from the fluorescence background noise (black).

Nature Neuroscience: doi:10.1038/nn.3646

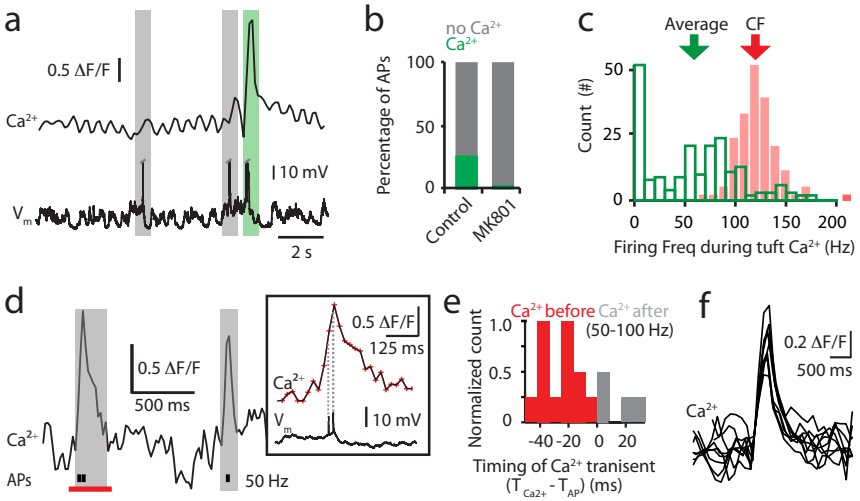

Supplementary Figure 2. Tuft Ca^{2+} transients are not from bAPs. Backpropagating action potentials (bAPs) cause Ca^{2+} influx into the dendrites of layer 2/3 pyramidal neurons in a distance-dependent manner (Svoboda et al, 1999; Waters et al, 2003). We tested the possibility that bAPs cause Ca^{2+} transients in tuft dendrites. **(a)** Tuft Ca^{2+} trace (top) and simultaneous somatic voltage (bottom). Bars highlight somatic APs with (green) and without (grey) associated tuft Ca^{2+} influx. APs truncated. **(b)** Only 26 ± 4 % of all somatic APs were associated with a Ca^{2+} transient in control tuft dendrites (n = 28). Although there were still spontaneous APs when all NMDA channels were blocked by internal MK801, there were no tuft Ca^{2+} transients illustrating the requirement of active NMDA channels (n = 6 dendrites). **(c)** Histogram of firing frequency recorded during tuft Ca^{2+} transients. The average firing frequency (60 ± 3 Hz) during tuft Ca^{2+} transients is considerably lower than the reported critical frequency (CF; red arrow) for evoking Ca^{2+} spikes in layer 2/3 pyramidal neurons (Larkum et al, 2007). Therefore bAPs alone could not evoke Ca^{2+} spikes which would cause Ca^{2+} influx into the tuft dendrites. **(d)** To investigate the timing of APs with dendritic Ca^{2+} activity**,** imaging frequency was increased to a maximum of 100 Hz. Typical tuft Ca^{2+} transients recorded at 50 Hz and somatic APs (black dashes). Grey bars, timing of Ca^{2+} transients compared to APs. Box, magnification of Ca^{2+} transient (top) and simultaneous somatic voltage (bottom) from the region marked with a red bar (left). Red markers on Ca^{2+} transient, data points (3 data points on the rising phase of the Ca^{2+} transient). **(e)** Histogram of the timing of Ca^{2+} transients recorded at 50-100 Hz compared to the timing of somatic APs. Timing was determined as the difference in time (ms) between the first data point on the rising phase of the tuft Ca^{2+} transient and the time at 10 % of the AP threshold for the first AP. On average, the onset of the tuft Ca^{2+} transient was 16 ± 6 ms before the somatic AP (n=17). **(f)** Overlay of spontaneous Ca^{2+} transients from a single tuft dendrite illustrating their stereotypic waveform (n=9). The amplitude of Ca^{2+} transients recorded in all dendrites were within one standard deviation of the mean.

Nature Neuroscience: doi:10.1038/nn.3646

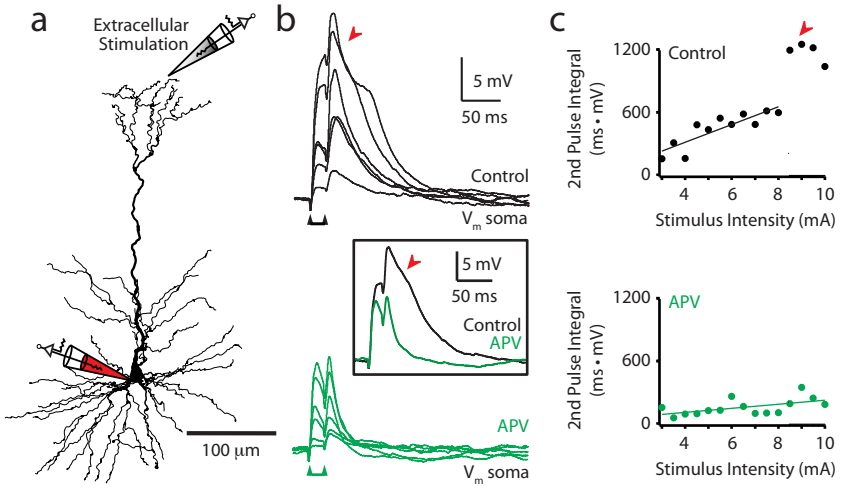

Supplementary Figure 3. NMDA spikes occur in tuft dendrites of layer 2/3 pyramidal neurons in vitro. NMDA spikes have been shown in the basal dendrites of layer 2/3 pyramidal neurons but not in the tuft dendrite. **(a)** Experimental paradigm. Somatic recordings were made from layer 2/3 pyramidal neurons filled with Alexa Fluor 594 (50 µM) to aid the placement of an extracellular stimulation pipette in close proximity to a tuft dendrite. **(b)** Sequentially increasing the intensity of paired pulses (2x 1 ms pulses at 50 Hz) applied to the tuft dendrite shown in (a) resulted in a supralinear voltage response (top; black) which was blocked by bath application of APV (100 µM; bottom; green). Inset, overlay of somatic voltage during supralinear stimulation during control (black) and APV (green). **(c)** Integral of the somatic voltage during sequential increase in stimulus intensity for the neuron shown in (a) and (b). Block of NMDA channels by APV significantly decreased the integral of the somatic voltage during a NMDA spike by on average 69 ± 10 % (2nd pulse; $n = 3$; $p < 0.05$; Data not shown). Data fitted with linear regression. Red arrows indicate suprathreshold response.

Nature Neuroscience: doi:10.1038/nn.3646

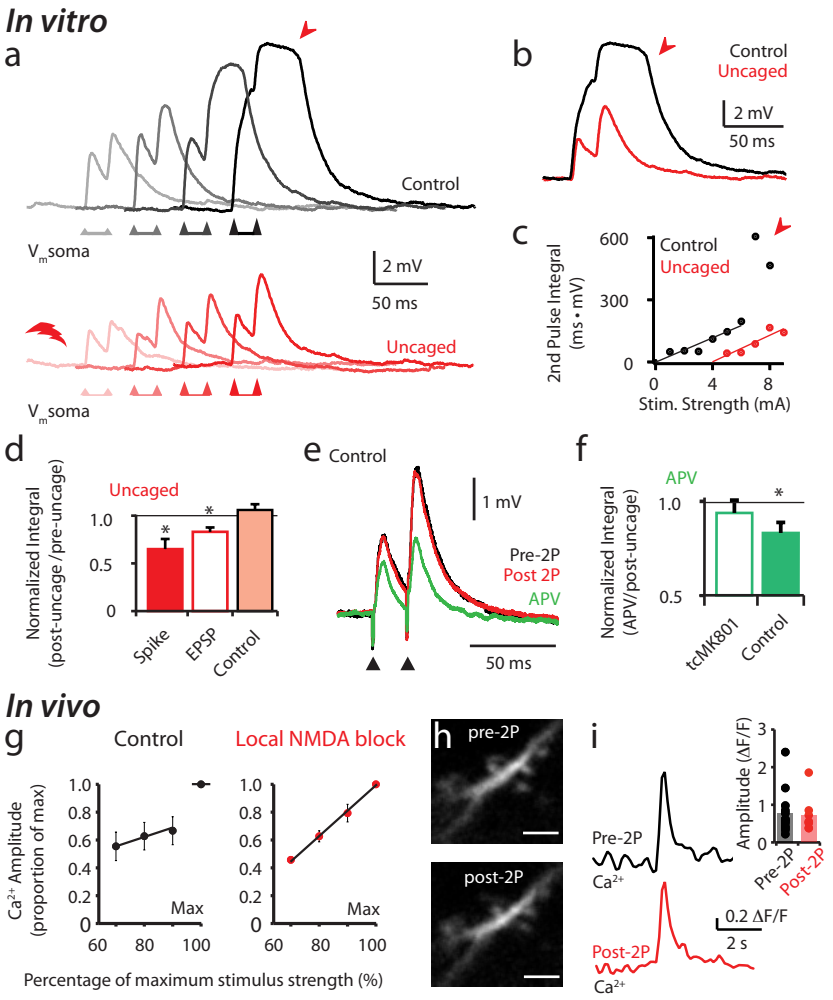

Supplementary Figure 4. Two-photon uncaging of tc-MK801 blocks NMDA spikes *in vitro* and *in vivo*. (a) Somatic voltage responses to sequentially increasing intensity of extracellular stimulation (2x 1 ms pulses at 50 Hz) before (black; top) and after (red; bottom) two-photon activation (710-730 nm) of a caged NMDA channel agonist (tc-MK801) at the stimulated branch *in vitro*. Arrow indicates a suprathreshold response. **(b)** Overlay of NMDA spike before (black) and after (red) uncaging tc-MK801 for the dendrite in (a). **(c)** Integral of the voltage response to increasing stimulus strength for the example shown in (a) and (b) before (black) and after (red) two-photon uncaging. Data fitted with linear regression. **(d)** Normalized integral after two-photon uncaging during a NMDA spike (red solid; n = 5), EPSP (red empty; n = 11) and control (laser exposure in neurons without tc-MK801; light red; n = 8). **(e)** Example of extracellularly stimulated potentials from a control neuron (no tc-MK801) before (black) and after (red) two-photon exposure (730 nm for ~3 min) and during bath application of APV (100 μM; green). **(f)** Normalized integral during bath application of APV after two-photon exposure in neurons filled with tc-MK801 (empty bar; n = 3) and in control (solid bar; n = 5). **(g)** Amplitude of Ca^{2+} responses to local extracellular stimulation (2x 1ms pulses at 50 Hz) normalized to the maximum evoked response before (black; left) and after (red; right) two-photon activation of the caged NMDA channel agonist tc-MK801 *in vivo* (n = 6 dendrites from 3 neurons). Uncaging tc-MK801 abolishes the supralinear response to increasing extracellular stimulation intensity. **(h)** Here, we show that exposure to two-photon excitation alone had no measureable adverse effects on the dendritic morphology or amplitude of Ca^{2+} transients. Dendritic morphology before (top) and after (bottom) two-photon laser exposure (690 nm, ~ 3 min). Scale bar, 2 μm. **(i)** Ca^{2+} transients before (black; top) and after (red; bottom) exposure to two-photon light (690 nm for ~3 min) from a control layer 2/3 pyramidal neuron filled with OGB1 and Alexa Fluor 594 (and not tc-MK801). Inset, there was no difference in the peak amplitudes of Ca^{2+} transients before (black) and after (red) exposure to two-photon excitation in control layer 2/3 pyramidal neuron dendrites. * indicates $p < 0.05$. Error bars represent S.E.M.

Nature Neuroscience: doi:10.1038/nn.3646

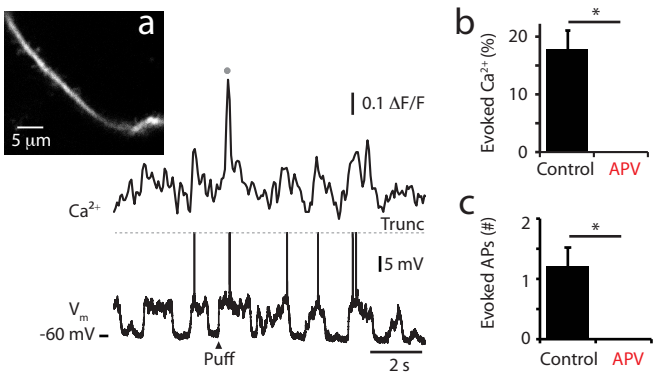

Supplementary Figure 5. Hindpaw airpuff reliably evokes dendritic and somatic responses which are dependent on NMDA receptors. Despite the different modes of hindpaw stimulation, brief electrical (Figure 2) and air puff stimulation (40 psi) evoked similar dendritic and somatic responses - approximately one action potential (AP) per stimulation and a dendritic Ca^{2+} response in approximately 20 % of stimulations. **(a)** Dendritic Ca^{2+} fluorescence (top) and somatic voltage (bottom) during airpuff stimulation of the hindpaw. Inset; two-photon image of the imaged tuft dendrite. **(b)** Percentage of hindpaw stimulation trials which resulted in a measurable Ca^{2+} transient during control (black; n=16) and NMDA block by cortical application of APV (red; n = 15). **(c)** Number of APs evoked by hindpaw stimulation during control (black; n = 5) and NMDA block by cortical application of APV (red; n = 15). Error bars represent S.E.M.

Nature Neuroscience: doi:10.1038/nn.3646

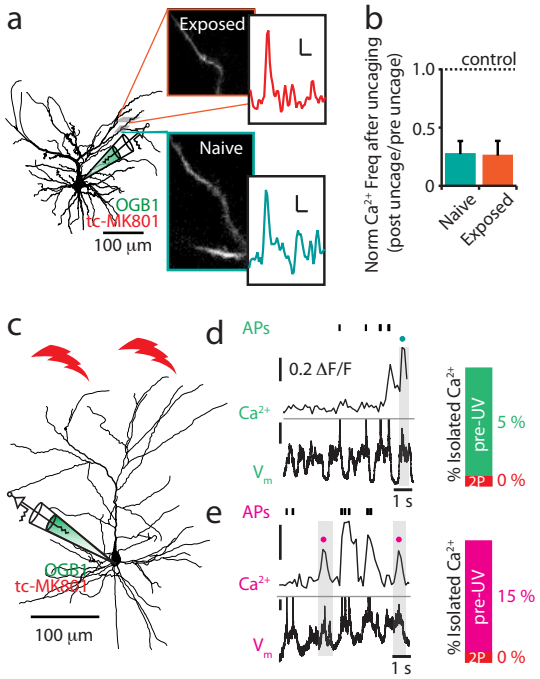

Supplementary Figure 6. Uncaging of tc-MK801 locally blocks NMDA channels. Here, we show that two-photon uncaging of tc-MK801 locally blocked NMDA channels by comparing the frequency of Ca^{2+} transients (a & b) and the occurrence of isolated Ca^{2+} transients (c-e) after subsequent uncaging at a neighboring branch. **(a)** Neurons were filled with the caged NMDA channel blocker tc-MK801. Ca^{2+} transients were recorded in both naive dendrites (no prior two-photon uncaging anywhere in the neuron; green; n = 8 dendrites) and exposed dendrites (neighboring dendrites had local NMDA channels blocked by uncaging tc-MK801; orange; n = 16 dendrites). Insets, control (pre uncaging) Ca^{2+} transients; scale, 0.2 ΔF/F, 1 s. The local block of NMDA channels by two-photon uncaging of tc-MK801 did not affect the frequency of spontaneous control Ca^{2+} transients in neighboring tuft dendrites (naive, 0.06 ± 0.02 Hz; exposed, 0.06 ± 0.03 Hz). **(b)** The frequency of spontaneous Ca^{2+} transients after local NMDA channel block (normalized to the control frequency) in naive dendrites (green) compared to exposed dendrites (orange). Note, block of NMDA channels does not affect the effectiveness of uncaging tc-MK801 in neighboring tuft dendrites. **(c)** Reconstruction of a L2/3 pyramidal neuron filled with tc-MK801. **(d) & (e),** Dendritic Ca^{2+} trace and simultaneous somatic voltage from two different tuft dendrites from the neuron shown in (c). Both dendrites have Ca^{2+} transients in the absence of somatic APs (indicated by colored dots). APs are indicated by dashes and are truncated. Both dendrites had Ca^{2+} transients (ie not correlated with a somatic AP) before (color) but not after (red) activation of tc-MK801 with two-photon laser. Error bars represent S.E.M.

Nature Neuroscience: doi:10.1038/nn.3646

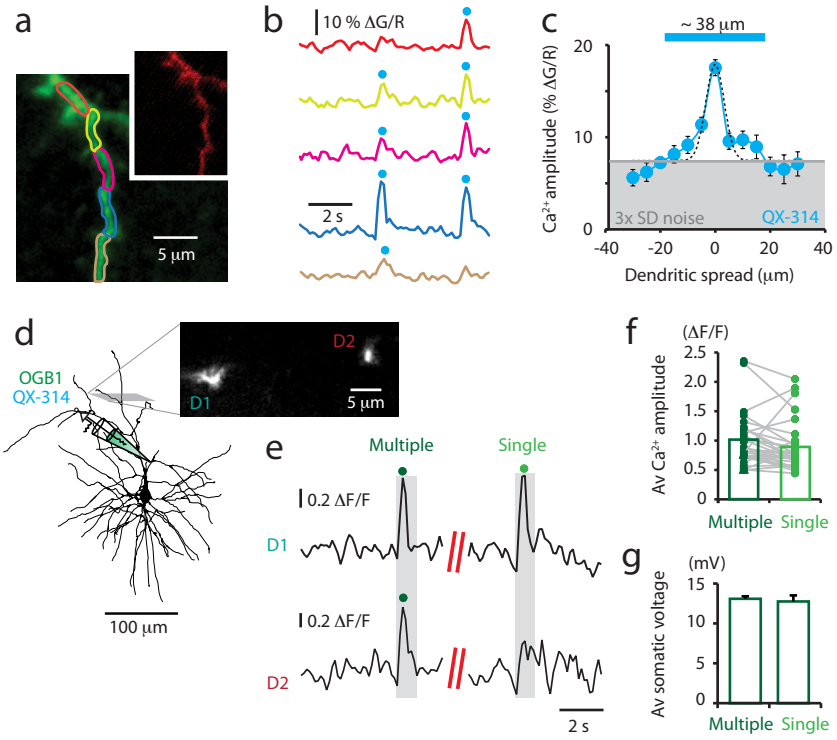

Supplementary Figure 7. Ca^{2+} transients in the presence of the Na^{+} channel blocker QX-314 are similar to control - they are spatially restricted and occur in both single and multiple branches. In theory, backpropagating APs from the cell body can invade the tuft dendrite and influence dendritic electrogenesis. We therefore tested whether tuft Ca^{2+} transients were influenced by somatic activity by adding the Na^{+} channel blocker QX-314 to the patch pipette. **(a)** Two-photon image illustrating a tuft branch with 5 µm regions of interest. Inset, red fluorescence. **(b)** Spontaneous Ca^{2+} transients from the dendrite shown in (a). Note the different spatial spread of the two transients. To compare different dendritic regions, transients are reported as ΔG/R. **(c)** Average Ca^{2+} transient spatial spread along dendritic tuft branches (5 µm regions of interest; n = 40 transients). Data fitted with Gaussian fit; dashed line. Grey line; threshold for events (> 3x standard deviation of the noise). **(d)** Reconstruction of layer 2/3 pyramidal neuron filled with QX-314 and two-photon image of two tuft dendrites. **(e)** Spontaneous Ca^{2+} transients which occurred in only one (single) or both (multiple) of the dendrites shown in (d). **(f)** Average peak amplitudes of the Ca^{2+} transients which occurred in single (light green) and multiple (dark green) branches (n = 508 transients in 41 branches). **(g)** Average somatic voltage during Ca^{2+} transients which occurred in single (light green) and multiple (dark green) branches (n = 9 branches) corrected for the increase in input resistance during QX-314 (see Fig. 3 and S9). Error bars represent S.E.M.

Nature Neuroscience: doi:10.1038/nn.3646

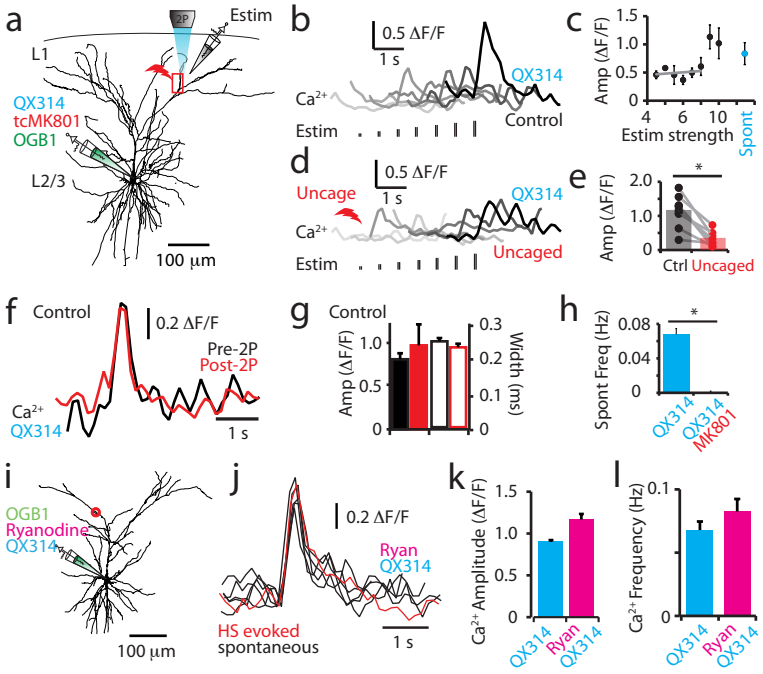

Supplementary Figure 8. Extracellular stimulation evokes large Ca^{2+} transients in tuft dendrites which is dependent on NMDA and not voltage-sensitive channels nor internal stores. Action potential (AP) initiation was blocked by including QX-314 in the patch pipette which completely or partially blocks Na^+, Ih, K^+ and Ca^{2+} channels (Perkins and Wong, 1995; Talbot and Sayer, 1996). **(a)** Reconstruction of a layer 2/3 pyramidal neuron illustrating the experimental design. Neurons were filled with QX-314 and the caged NMDA channel blocker tc-MK801, and an extracellular stimulating pipette was placed in close proximity to a branch of interest. **(b)** Overlay (spatially shifted for display purposes) of Ca^{2+} transients in response to increasing stimulus intensity from the tuft dendrite boxed in (a). **(c)** Average Ca^{2+} transient amplitude during focal extracellular stimulation of increasing intensity (black, n = 7) and during spontaneous activity (blue; n = 7). Linear regression for subthreshold responses is shown by grey line. **(d)** Overlay (spatially shifted for display purposes) of Ca^{2+} transients in response to increasing stimulus intensity after (bottom) block of NMDA receptors by two-photon (690 nm) uncaging of tc-MK801 from the boxed tuft dendrite in (a). **(e)** The evoked Ca^{2+} transient amplitude to the same suprathreshold stimulation strength was significantly larger before (black) than after (red) block of NMDA receptors by two-photon (690 nm) uncaging of tc-MK801. **(f)** Two-photon laser alone doesn't affect Ca^{2+} activity. Here, we show that exposure to two-photon excitation alone had no measureable adverse effect on the amplitude or width of Ca^{2+} transients in neurons filled with QX-314. Ca^{2+} transients before (black) and after (red) exposure to two-photon light (690 nm for ~3 min) from a layer 2/3 pyramidal neuron filled with QX-314 (and not tc-MK801). **(g)** Peak amplitudes (left) and width (right) of Ca^{2+} transients before (black) and after (red) exposure to two-photon excitation from control layer 2/3 pyramidal neurons (n = 9). **(h)** Average frequency of spontaneous tuft Ca^{2+} transients during QX-314 alone (blue; n=40 dendrites) and QX-314 and MK801 (red; n=11 dendrites) in the patch pipette. **(i)** In addition to synaptic input, large Ca^{2+} events in the apical dendrites of layer 2/3 neurons have also been shown in vitro to be due to Ca^{2+} release from ryanodine-sensitive intracellular stores (Larkum et al, 2003). We therefore tested whether the large Ca^{2+} events we measured in vivo were ryanodine sensitive. Reconstruction of layer 2/3 pyramidal neuron filled with ryanodine (10 µM) and QX-314 (1 mM). **(j)** Spontaneous (black) and evoked (hindlimb stimulation; red) Ca^{2+} transients recorded from the neuron shown in (i). The location of the imaged tuft dendrite is indicated by a red circle in (i). **(k)** Average peak amplitude and **(l)** frequency of the Ca^{2+} transients in neurons filled with QX-314 alone (blue; n = 465 transients from 8 dendrites) and both QX-314 and ryanodine (fuchsia; n = 117 transients from 42 dendrites). * $p < 0.05$. Error bars represent S.E.M.

Nature Neuroscience: doi:10.1038/nn.3646

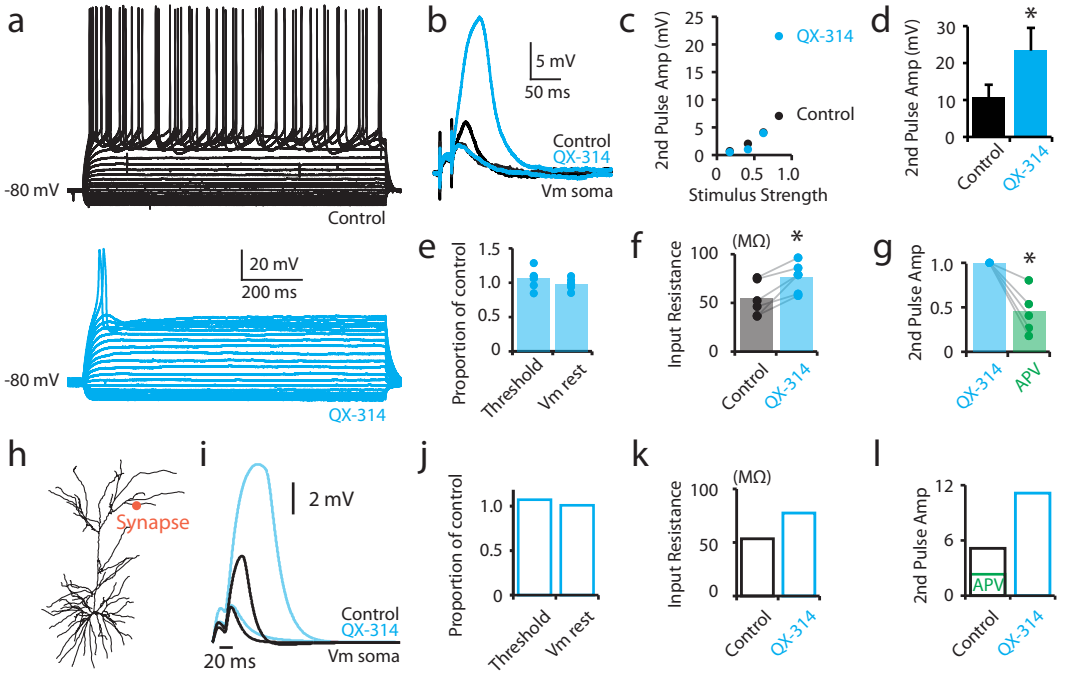

Supplementary Figure 9. QX-314 increases the amplitude of the somatic voltage during NMDA spikes in tuft dendrites of layer 2/3 pyramidal neurons *in vitro* and *in silico*. Intracellular application of QX-314 blocks Na^+ channels as well as partially blocks Ca^{2+}, Ih and K^+ channels (Perkins and Wong, 1995; Talbot and Sayer, 1996). The effect of QX-314 on NMDA spikes was tested using somatic recordings from layer 2/3 pyramidal neurons which were initially patched with control intracellular solution and then repatched with intracellular solution containing QX-314. Neurons were filled with Alexa Fluor 594 (50 µM) to aid the placement of an extracellular stimulation pipette in close proximity to a tuft dendrite. **(a)** Somatic voltage response to somatic current step injections (100 pA steps) before (black) and after (blue) QX-314. Note the lack of action potentials in the presence of QX-314. **(b)** Sequentially increasing the intensity of paired pulses (2x 1 ms pulses at 50 Hz) to the tuft dendrite resulted in a supralinear voltage response both before (black) and after QX-314 (blue). A subthreshold and suprathreshold response is shown for each condition. **(c)** Amplitude of the somatic voltage during sequential increase in stimulus intensity for the example shown in (b). **(d)** QX-314 significantly increased the amplitude of the voltage response by approximately two-fold (2nd pulse; $n = 5$; $p < 0.05$). **(e)** There was no significant influence of QX-314 on the stimulus intensity (threshold) required to evoke a spike ($n = 5$) nor the resting membrane potential ($n = 6$). **(f)** However, QX-314 significantly increased the input resistance by on average 48 ± 15 % ($n = 6$). **(g)** Bath application of the NMDA channel agonist APV (50 µM; bottom; green) significantly decreased the voltage response. **(h)** The effects of intracellular QX-314 on synaptic input (location; orange dot) was modeled by completely or partially blocking Na^+, Ih, K^+ and Ca^{2+} conductances (see supplemental methods). **(i)** Subthreshold and suprathreshold somatic responses to increasing NMDA/AMPA input in control (black) and QX-314 (blue) simulations at the synapse shown in (h). Note, the computer simulations are comparable to the experimental data in (b). In the presence of QX-314, the computational model shows no effect on threshold or resting membrane potential **(j)**, an increase in the input resistance **(k)** and an increase in the amplitude of the second pulse of the paired pulse stimulation which was decreased during bath application of APV in control **(l)**. These computer simulation results are comparable to the *in vitro* data shown in (a) - (g) and the increase in voltage during QX-314 can be entirely explained by the decrease in input resistance. * indicates $p<0.05$. Error bars represent S.E.M.

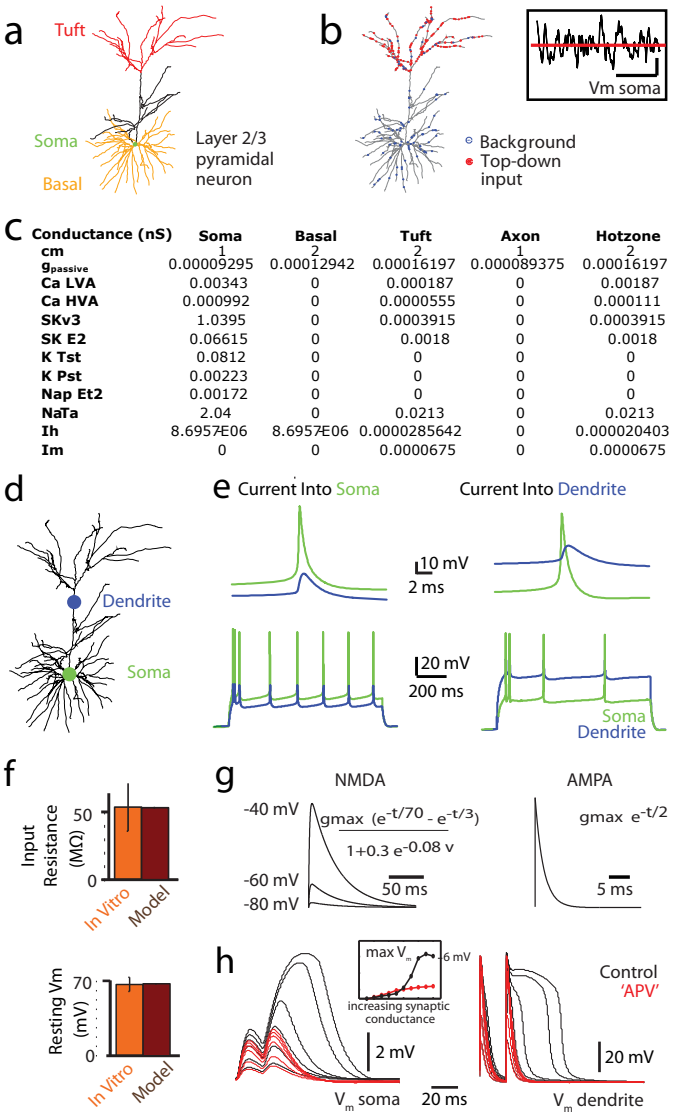

c

Conductance (nS)	Soma	Basal	Tuft	Axon	Hotzone
	1	2	2	1	2
cm					
$g_{passive}$	0.00009295	0.00012942	0.00016197	0.000089375	0.00016197
Ca LVA	0.00343	0	0.000187	0	0.00187
Ca HVA	0.000992	0	0.0000555	0	0.000111
SKv3	1.0395	0	0.0003915	0	0.0003915
SK E2	0.06615	0	0.0018	0	0.0018
K Tst	0.0812	0	0	0	0
K Pst	0.00223	0	0	0	0
Nap Et2	0.00172	0	0	0	0
NaTa	2.04	0	0.0213	0	0.0213
Ih	8.6957E06	8.6957E06	0.0000285642	0	0.000020403
Im	0	0	0.0000675	0	0.0000675

Supplementary Figure 10. Details of the layer 2/3 computational model. (a) A reconstructed L2/3 pyramidal neuron from the experimental part of this study was used for simulations in NEURON. **(b)** Top-down synaptic inputs (red) were placed with uniform probability distribution across the tuft dendrites and a further 100 synaptic inputs were distributed with uniform probability across the entire neuron to simulate background synaptic input (blue). Inset, background membrane potential. Red line: 17.3 mV from rest. Scale, 1 mV; 150 ms. **(c)** Table of conductance values used in the simulated neuron. All values are in units of nS. **(d)** A reconstructed L2/3 pyramidal neuron. **(e)** Computer simulations of the voltage response at the soma (green) and dendrite (blue) during current injection (1 s) into the soma (left) and dendrite (right) for the modeled neuron shown in (d). **(f)** Comparison of vitro experiments (n = 6) and the model neuron for input resistance and resting membrane potential. Error bars are standard deviation. **(g)** (left) Nonlinear NMDA conductance used in the model. Note that the conductance is a function of the local membrane potential. Plots are shown at –40, –60, and –80 mV. (Right) Linear AMPA conductance used in the model. Note that the AMPA conductance is voltage independent. **(h)** Simulated voltage response to paired pulse stimulation (50 Hz) with increasing intensity with (red) and without (black; 'APV') NMDA conductance recorded at the soma (left) and at the site of stimulation (tuft dendrite; right). Inset, maximum voltage response at the soma as synaptic conductance increases. The non linearity in the control condition establishes the event as an NMDA spike, as described in previous work (Schiller et al., 2000, Schiller and Schiller, 2001, Spruston and Kath, 2004, Rhodes, 2006, Major et al., 2008, Larkum et al., 2009, Polsky et al., 2009, Lee, 2012).

Nature Neuroscience: doi:10.1038/nn.3646

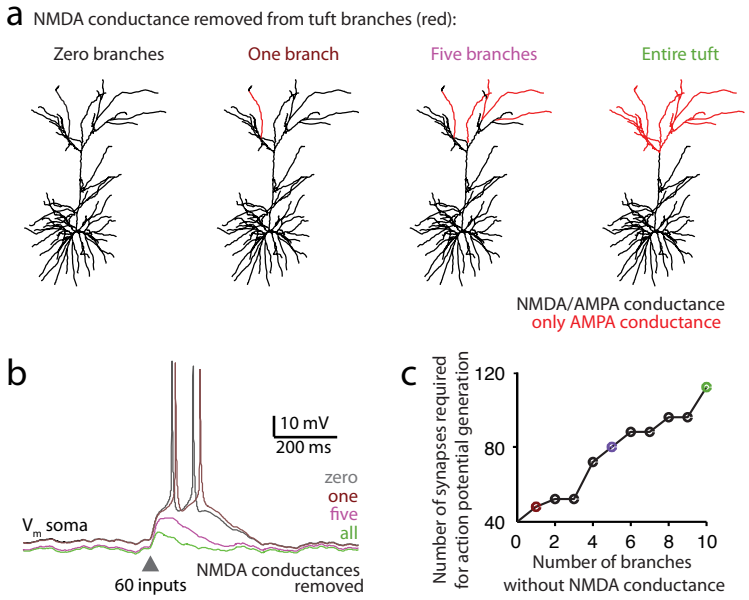

Supplementary Figure 11. Blocking distributed NMDA conductances in the majority of the tuft affects AP generation. The experimental data showed that locally blocking NMDA channels in a single tuft branch does not affect somatic action potentials (APs). To further investigate this, we used computer simulations in the NEURON simulation platform to manipulate the extent of the tuft experiencing NMDA block and measure the resulting effect on neuronal output. Top-down synaptic inputs were randomly distributed across the tuft dendrites and a further 100 synaptic inputs were distributed with uniform probability across the entire neuron to simulate background synaptic input (see Fig. S10). **(a)** A model layer 2/3 pyramidal neuron had NMDA conductances blocked in varying numbers of tuft branches. Synaptic input was randomly distributed for each trial and branches shown in red had both background and top-down NMDA conductances blocked. **(b)** Membrane potential traces in response to 60 synaptic inputs randomly distributed onto the tuft dendrite in neurons where NMDA conductances were removed from no (grey), one (brown), five (fuchsia) and all (green) tuft branches. During this simulation, NMDA block in five tuft dendrites is sufficient to substantially change neuronal output. **(c)** The total number of synapses needed to generate an AP compared to the number of branches with NMDA conductances removed. Colored dots refer to data shown in (b).

Nature Neuroscience: doi:10.1038/nn.3646